Graphene Materials

International Edition: DOI: 10.1002/anie.201511064
German Edition: DOI: 10.1002/ange.201511064

# A Phytic Acid Induced Super-Amphiphilic Multifunctional 3D Graphene-Based Foam

*Xinhong Song, Yiying Chen, Mingcong Rong, Zhaoxiong Xie, Tingting Zhao, Yiru Wang, Xi Chen,* and Otto S. Wolfbeis*

***Abstract:*** *Surfaces with super-amphiphilicity have attracted tremendous interest for fundamental and applied research owing to their special affinity to both oil and water. It is generally believed that 3D graphenes are monoliths with strongly hydrophobic surfaces. Herein, we demonstrate the preparation of a 3D super-amphiphilic (that is, highly hydrophilic and oleophilic) graphene-based assembly in a single-step using phytic acid acting as both a gelator and as a dopant. The product shows both hydrophilic and oleophilic intelligence, and this overcomes the drawbacks of presently known hydrophobic 3D graphene assemblies. It can absorb water and oils alike. The utility of the new material was demonstrated by designing a heterogeneous catalytic system through incorporation of a zeolite into its amphiphilic 3D scaffold. The resulting bulk network was shown to enable efficient epoxidation of alkenes without prior addition of a co-solvent or stirring. This catalyst also can be recovered and re-used, thereby providing a clean catalytic process with simplified work-up.*

The wetting behavior of solid surfaces by a liquid represents an important aspect of surface chemistry.[1–4] Surfaces that possess super-amphiphilicity (that is, where contact angles for water and oil approach 0°) have a wide range of applications.[1–7] The current toolbox for the fabrication of amphiphilic materials includes methods such as selective etching of solid or polymer templates, self-assembly of block copolymers, photogeneration, and plasma treatment.[1–7] Although implemented in some studies, these methods have limitations that are mainly due to the requirement for multistep procedures for implementation, the poor resistance to harsh conditions, or to limitations in substrate size.

Three-dimensional (3D) graphene-based materials with tuned surface properties have drawn increasing attention for catalysis, energy conversion, and environmental applications.[8–16] The wettability of graphene assemblies play a critical role in not only governing the interaction between graphenes and their environment, but also directly impacting many of their properties, such as wetting,[17,18] adhesion,[19] and electronic properties.[20,21] Most 3D graphene assemblies are based on the use of graphene oxide (GO),[22,23] which features hydrophobic aromatic domains and hydrophilic domains carrying various kinds of oxygen functions. However, owing to its strong π-stacking and hydrophobic interactions, sheets of reduced GO (rGO) tend to irreversibly form agglomerates or even restack to form graphite. Thus, the assembly of GO usually leads to hydrophobic or super-hydrophobic products.[10–15] To our knowledge, there is no report so far on a super-amphiphilic 3D graphene-based architecture that would show both super-hydrophilic and super-oleophilic properties.

A major challenge in the design of amphiphilic 3D graphene-based assembly requires a microstructure containing hydrophilic and oleophilic domains that form a network of open super-wetting capillaries.[1–7] To impart 3D graphene assemblies with wettability, we perceived phytic acid (*myo*-inositol 1,2,3,4,5,6-hexakisphosphate, PA; Scheme 1) to be a well-suited material. PA is eco-friendly, renewable, and an abundant biomass that is readily obtained from grains.[24–26] The six phosphate groups provide a variety of viable cross-linking sites that may "stitch" two or more sheets of GO to form 3D assemblies. Herein, we report a template-free, single-step method for the scalable fabrication of 3D graphene-based foam (PAGF) possessing super-amphiphilicity.

The preparation of the PAGF is outlined in Scheme 1. It comprises the hydrothermal reaction[27] of GO with PA. In this process, PA plays multiple roles in not only reducing the twisted GO sheets to assemble into the compact 3D porous foam with good structural stability, but also introducing many new functional groups, such as inositol triphosphate and phosphoric acid, which can act as hydrophilic functional groups.

[*] X. H. Song, Y. Y. Chen, M. C. Rong, Prof. Y. R. Wang, Prof. Dr. X. Chen
Department of Chemistry
College of Chemistry and Chemical Engineering
Xiamen University
Xiamen 361005 (China)
E-mail: xichen@xmu.edu.cn
Prof. Dr. X. Chen
State Key Laboratory of Marine Environmental Science
Xiamen University
Xiamen 361005 (China)
Prof. Dr. O. S. Wolfbeis
University of Regensburg
Institute of Analytical Chemistry, Chemo- and Biosensors
93040 Regensburg (Germany)
Prof. Dr. Z. X. Xie
State Key Laboratory of Physical Chemistry of Solid Surfaces
Collaborative Innovation Center of Chemistry for Energy Materials
and
College of Chemistry and Chemical Engineering, Xiamen University
Xiamen 361005 (China)
T. T. Zhao
Department of Planning
Xiamen Huaxia University
Xiamen 361024 (China)

Supporting information for this article, including the syntheses characterizations, can be found under http://dx.doi.org/10.1002/anie.201511064.

 © 2016 Wiley-VCH Verlag GmbH & Co. KGaA, Weinheim 


***Scheme 1.*** Fabrication of the 3D graphene foam (PAGF).

The interactions between GO sheets and PA molecules are governed by various forces, but hydrogen bonding is likely to play the main role. PA is viable for capturing the GO sheets because its six phosphate groups are located on either side of the cyclohexane ring. One on hand, the GO sheets can be readily reduced to rGO with partial restoration of the conjugated structure through hydrothermal reduction. On the other hand, the obtained rGO are chemically modified by PA. PA facilitates rapid proton transport through association or dissociation,[28] with the phosphate groups acting as either proton acceptors or donors. This is highly beneficial in terms of forming dynamic hydrogen bonds, and also increases the probability of simultaneous interaction with several rGO sheets. Figure 1a shows the morphology of the resulting PAGF hydrogel containing 2 mg mL$^{-1}$ of GO but varying fractions of PA.

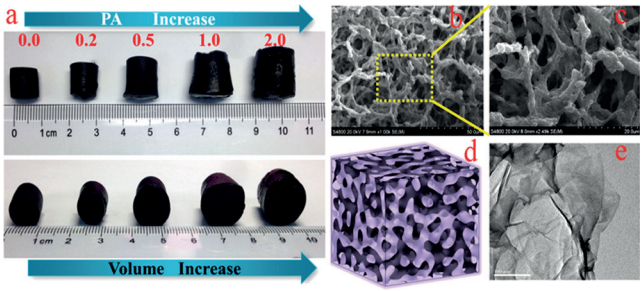


***Figure 1.*** a) Morphology of the products prepared using the hydrothermal reaction of GO dispersion (2 mg mL$^{-1}$) with a different initial volume of PA (0–2 mL). b,c) SEM images of the PAGF in varying magnification. d) 3D porous structure of the PAGF. e) TEM image of the PAGF.

The volume of PAGFs increased as the fraction of added PA was increased. However, if more than 3 mL of the PA solution were added to the GO solution, the resulting mass became soft and the GO/PA mixture did not form a stable hydrogel (Supporting Information, Figure S1). This indicates that the high coverage of the surface of GO with PA reduces the number of sites for cross-linking between GO sheets. The microstructure of PAGFs fabricated by different ratios of PA and GO are shown in Figure S2. Because the PAGF formed by 0.5 mL of PA had the best adsorption capacity (see below), the following PAGFs refer to the ones fabricated using 0.5 mL PA unless otherwise specified.

Fortunately, PA is a readily available resource. This, combined with the simplicity of the assembly process, allows for easy control of the shape and size of the product. For example, the PAGF cylinder of hydrogel can be sliced into pieces to obtain a round disk shape for further use (Figure S3). Scanning electron microscopy (SEM; Figures 1b,c) revealed the morphology of the 3D PAGF. The twisted nanosheets were stacked and formed a rough network with interpenetrated nano- and micropores, thus forming a "bird's nest"-like structure. Figure 1d provides an illustration of the three dimensional porous microstructure of PAGF. The molecular building blocks (PA and GO) favor the formation of interconnected network because each PA molecule can interact with several rGO sheets to form a branched microstructure. Transmission electron microscopy (TEM; Figure 1e) further illustrated the wrinkled and even folded structure of the 3D network.

Most surprisingly, however, is the finding that this PAGF possesses a kind of super-amphiphilicity. Figures 2a–b demonstrate its capability of absorbing both water solutions and hydrophobic oil. This contrasts with previously reported 3D graphene assemblies, which were either mono-hydrophobic[10–15] or mono-hydrophilic.[16]

When pushing pieces of the PAGF over drops of water and oil (Figure 2a; Movie S1), it rapidly adsorbed both water and oil (which was dyed with Sudan III for better visibility). For comparison, Figure 2b shows complete sequential adsorption of water and oil if a piece of PAGF was vertically pushed over drops of water and oil, respectively (Movie S2).

The surface roughness of the PAGF also affects wettability, and therefore the surface was analyzed using 3D laser scanning confocal microscopy. Figure 2c revealed a rough surface that consists of peaks and valleys. The high degree of surface fluctuation led to a mean roughness ($R_a$)[29,30] of about 19.70 ± 0.3 μm. Next, the chemical composition of the PAGF was investigated. The Fourier transform infrared spectra (Figure 2d) were different from those of graphene foam (GF) and of GO in showing new bands peaking at 1161, 1057, 1003, and 886 cm$^{-1}$. These can be attributed to the stretching vibrations of P=O, P–O–C (phosphate ester group), P–O, and P–O–H, respectively.[31,32] The peaks appearing around 510 cm$^{-1}$ were attributed to the deformation vibration of $PO_4$.[32] Compared to GF, the new strong peaks at around 3415 and 1610 cm$^{-1}$ indicate the strong hygroscopic character of PAGFs. The X-ray diffraction (XRD) pattern of the PAGF showed a broad diffraction peak at 24.9°, which was assigned to the (002) plane of stacked graphene sheets in the XRD pattern (Figure S4). X-ray photoelectron spectroscopy (XPS) revealed a graphitic C1s peak at around 284.8 eV and a strong O1s peak at around 532.7 eV. This confirmed the presence of hydrophilic oxygen-containing groups, such as hydroxy/epoxy groups (Figure 2e). XPS also showed the characteristic P2s and P2p peaks at 191 and 134.5 eV, thereby providing

 © 2016 Wiley-VCH Verlag GmbH & Co. KGaA, Weinheim 

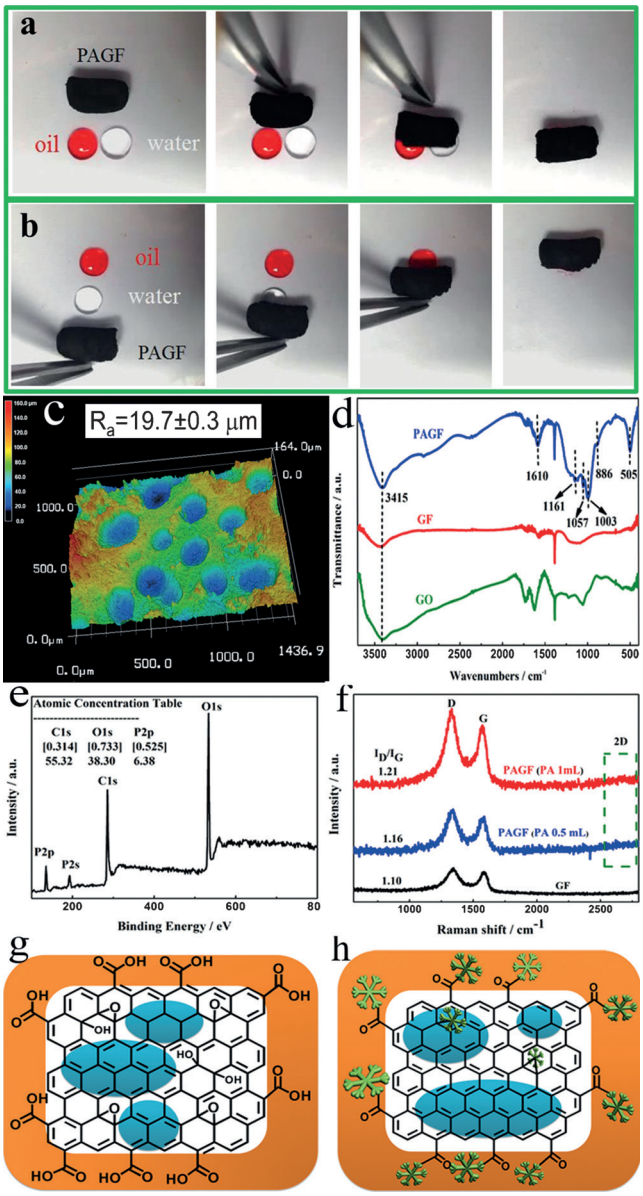


***Figure 2.*** Photos of a) the side-by-side simultaneous adsorption, and b) the sequential adsorption of water and oil by the PAGF. Also see Movies S1 and S2 in the Supporting Information. c) Determination of the surface roughness of the PAGF. d) FTIR spectrum. e) XPS spectrum. f) Raman spectra of the PAGF with different initial amounts of PA and the spectra of the GF, where D, G, and 2D denote the characteristic D band, G band, and 2D band of graphene. g) Structural model of GO sheets. h) Structural model of PAGF showing hydrophilic PA molecules mostly attached at the edges of the modified graphene, and graphitic domains on its basal plane.

evidence for the successful integration of PA. High-resolution XPS of C, O, P, and their deconvolution is shown in Figure S5. The Raman spectrum, in turn, revealed the typical G band at about 1580 $cm^{-1}$, and the D band at about 1340 $cm^{-1}$ (Figure 2 f). The ratio of the intensities of the D and G bands ($I_D/I_G$) can be utilized [33,34] to gauge the degree of structural disorder and defects. The relatively large amount of phosphate groups originating from PA reduce the relative number of six-membered aromatic rings, and thus increase the intensity of the D band while decreasing that of the G band. As a result, the ratio $I_D/I_G$ is enlarged by 10% (from 1.10 to 1.21). This suggests that by increasing the initial concentration of PA, the number of phosphate groups can be increased which would cause an increase in disorder. More information about the structure and properties of the 3D PAGF studied by the rheological measurements are shown in the Supporting Information (Figure S6).

GO sheets are assumed to carry their carboxy groups at the edges, while the epoxy and hydroxy groups and graphitic domains reside in the basal plane (Figure 2 g).[22,23] Upon hydrothermal treatment, GO sheets are reduced to rGO sheets that contain more hydrophobic domains.[23] Overlapping (or even coalescent) rGO sheets are stabilized by the presence of PA, most probably at the edges (Figure 2 h). This prevents the rGO sheets to irreversibly agglomerate or restack. The large fraction of phosphate groups also compensates for the loss of hydroxy groups that occurred as a result of the reduction of GO. Therefore, the unique composition of hydrophilic oxygenated functional groups and hydrophobic aromatic domains of the PAGF endowed it with unique amphiphilic properties.

The formation of a monolithic 3D interconnected and rough network resembles a 3D capillary imbibition phenomenon[3–7] of the spontaneous invasion of liquid into the textured material. Figures 3 a–c show a PAGF pellet that was placed on the desk and then horizontally moved towards a drop of water. The pellet virtually acts like a magnet by attracting and adsorbing the water instantaneously, leaving the side of the surface dry (Movie S3). This phenomenon is also observed if the water drop is being replaced by a drop of oil. Evidently, the amphiphilic structure endows the surface with amphiphilicity, while the capillary forces cause a wicking action. The combination of these two factors is assumed to cause the observed super-wetting property of the PAGF.

To further examine the wettability of the PAGF, videos of contact angle measurements were acquired at a capture speed of 20 frames per second. A droplet of liquid was deposited on the surface of the PAGF where it first rapidly spread over the contact area, and then spontaneously penetrated into the porous structure. Figures 3 d–e show how a droplet of water/oil spread on the PAGF, while the water contact angle approached 0° within 1.0 s (Movie S4). Similarly, when depositing an oil droplet, the contact angle approached 0° within 1.2 s (Movie S5), again indicating the super-amphiphilicity of the PAGF. Water spread faster than oil, presumably as a result of the difference in viscosities.

Water can be spread on the surface of only a few nonporous materials. These include glass, gold, selected oxides ($TiO_2$, ZnO), selected self-assembled surfaces with hydroxy functionalities (OH, COOH), and spreading only happens if the materials are freshly fabricated and their surfaces are very clean.[3,7] Their strong hydrophilicity is usually a short-lasting effect[7] that is strongly compromised by contaminants. In contrast, the PAGF presented here retains its super-hydrophilicity even after storage in a glass tube for a year. Moreover, even dehydrated PAGF can be readily rehydrated (Figure 3 f).


© 2016 Wiley-VCH Verlag GmbH & Co. KGaA, Weinheim

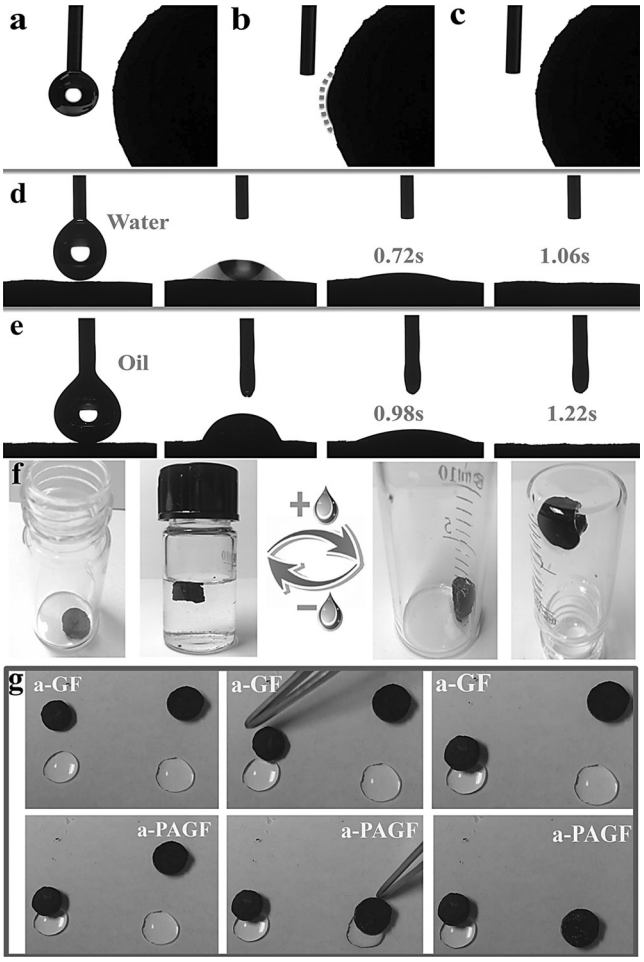


***Figure 3.*** a–c) The imbibition of water into the PAGF (also see Movie S3). d) The spreading process of a droplet of water (2 μL) on the PAGF surface (Movie S4). e) The spreading process of a droplet of oil (2 μL) on the PAGF surface (Movie S5). f) Photos of the PAGF and its dehydrated form which can be switched during several turns of dehydration and hydration. g) Photos of the adsorption process of water by a-GF and a-PAGF (Movie S7).

The particular feature of this easily accessible and ecofriendly material of soaking oils and water alike makes it a superb sorbent for environmental remediation. The comparison among the adsorption capacity of PAGFs fabricated by different ratios of PA and GO is shown in Figure S7, from which we found the PAGF (0.5 mL PA) has the highest adsorption capacity towards both water and oil. The adsorption capacity and the recyclability of PAGF (0.5 mL PA) towards various kinds of liquids (water, commercial petroleum products, fats, aromatic compounds, hydrocarbons, and chloroform) are shown in Figures S8 and S9, and Movie S6. We also tested whether the super-amphilicity, especially the hydrophilicity of PAGFs, may be affected by temperature. Conventional graphene foam becomes extremely hydrophobic after annealing it at 1000 °C for 3 h (named "a-GF"). It was found, however, that the PAGF after annealing (named as "a-PAGF") retains its strong affinity to water (Figure 3 g and Movie S7).

The amphiphilic character of PAGFs has an additional attractive feature with respect to heterogeneous catalysis where the immiscibility and thermal instability of catalytically formed products can adversely affect work-up and yields.[35–38] For example, the epoxidation of olefins with hydrogen peroxide ($H_2O_2$) using heterogeneous catalysts is an environmentally friendly route for preparation of epoxides.[39–41] $H_2O_2$ is generally supplied as an aqueous solution, but this slows down its transfer to hydrophobic olefins contained in an organic phase. Commonly used catalyst particles in such epoxidations include titanium silicalite-1 (TS-1),[42–45] but they do not interact well with water-immiscible substrates unless modified in several chemical steps. We show here that the 3D PAGF represents a powerful heterogeneous support system for use in the catalytic epoxidation of alkenes with aqueous $H_2O_2$ without the need for a co-solvent. The catalyst TS-1 was incorporated into the PAGF network already during its hydrothermal preparation to obtain a catalytically active graphene monolith (PAGF-TS). Neither the interconnected porous structure nor the zeolite structure was destroyed during the process (Figure S10).

The PAGF-TS was then used for catalytic epoxidation of 1-octene without adding a co-solvent. Figure 4 a shows photographs of three pieces of PAGF-TS placed in a) 1-octene, b) 30 % aqueous $H_2O_2$, and c) a biphasic system composed of

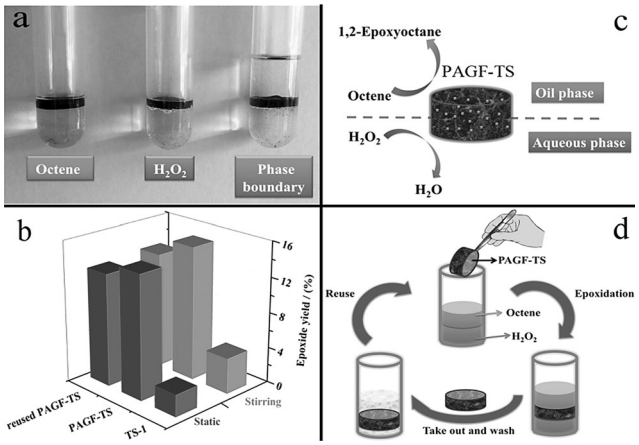


***Figure 4.*** a) Photograph of the PAGF-TSs pellets suspended in octene, aqueous $H_2O_2$, and at the octane/$H_2O_2$ interface. b) The effect of various reagents on the yield of epoxide. c) Proposed action of the interface catalyst (PAGF-TS). d) Illustration of the reusability of the PAGF-TS catalyst. The reactions were carried out with TS-1, PAGF-TS, and recycled PAGF-TS.

1-octene and aqueous $H_2O_2$. The PAGF-TS pellets quickly suspend themselves in octene and in aqueous $H_2O_2$. If placed in the biphasic system, the PAGF-TS assume a position at the interface between the two liquids. In comparison, the original TS-1 particles remain dispersed in the aqueous phase, as can be expected based on their hydrophilicity (Figure S11). In a typical experiment, octene (4 mL), 30 % aqueous $H_2O_2$ (2 mL), and the catalyst PAGF-TS (TS-1; 50 mg) were placed in a glass tube, and the reaction was performed with or without stirring for 12 h at 60 °C.

 © 2016 Wiley-VCH Verlag GmbH & Co. KGaA, Weinheim 

GC-MS analysis indicates that 1,2-epoxyoctane is the sole reaction product, and conceivable by-products such as 2-octanone, 1-octanol, 2-octanol, or 1,2-octanediol were not found (Figure S12). Evidently, the use of PAGF-TS enables a clean catalytic process, with minimal formation of by-products and simple work-up. It is noted that the TS-1 zeolite was exemplary as an easily available catalyst, and that the reaction conditions were not optimized. Further studies on improving the catalytic activity by generating more effective four-coordinated titanium species for use in the catalytic system are underway.

Figure 4b shows that the yield of 1,2-epoxyoctane when using PAGF-TS as a catalyst is much higher than when using TS only, or comparable to previously reported yields.[40,42,45] Obviously, the use of PAGF-TS as a support increases the interfacial area to result in a catalytic activity much higher than that of parent TS-1. The course of reaction (Figure 4c) may involve catalytic oxidation by $H_2O_2$ in the hydrophilic domains in aqueous solution, while the hydrophobic areas favor the transport and availability of the organic component. After completion of the reaction, the catalyst can be simply taken out and recycled by washing and drying it (Figure 4d). When re-used under the same conditions, it displays virtually the same activity (Figure 4b).

In summary, we describe a facile route for the preparation of 3D graphene-based foams possessing unique super-amphiphilicity. The synergy resulting from interaction between the highly hydrophilic PA (a biomass molecule) and the highly hydrophobic graphene results in a surprisingly large effect on surface wetting. The so-far unmatched amphiphilicity is ascribed to a comparably rough surface with microstructured domains consisting of hydrophobic aromatic and hydrophilic phosphate nanodomains. By incorporating an epoxidation catalyst as an additional functional element into the PAGF network, a catalyst is obtained that freely positions itself at the interface of an aqueous–organic binary system. This catalyst can efficiently catalyze the epoxidation of octene even without stirring or the need for a co-solvent to drive phase transfer. The catalyst is also readily recycled and can be re-used. In our view, this amphiphilic 3D graphene foam represents a significant step forward in the design of new heterogeneous catalysts. The unique super-amphiphilicity of this 3D graphene-based assembly is likely to lend itself to the design of multifunctional materials with improved performance in environmental remediation, heterogeneous catalysis, electro-wetting, and in chemical sensing and biosensing.

## Acknowledgements

This research was financially supported by the National Nature Scientific Foundation of China (No. 21375112), the Program for Changjiang Scholars and Innovative Research Team in University (No. IRT13036), the Foundation for Innovative Research Groups of the National Natural Science Foundation of China (Grant No. 21521004), the Marine high-tech industry development projects of Fujian Province (No. 2015-19), and the Major Projects Science and Technology of Fujian Province (No. 2011YZ0001-1). We would also like to extend our thanks to Prof. Bin Ren for his valuable suggestions, and Prof. John Hodgkiss of the University of Hong Kong for his assistance with English.

**Keywords:** 3D graphene foams · heterogeneous catalysis · phytic acid · super-amphiphilic

**How to cite:** *Angew. Chem. Int. Ed.* **2016**, *55*, 3936–3941
*Angew. Chem.* **2016**, *128*, 4004–4009

[1] R. Blossey, *Nat. Mater.* **2003**, *2*, 301–306.
[2] T. Sun, L. Feng, X. Gao, L. Jiang, *Acc. Chem. Res.* **2005**, *38*, 644–652.
[3] X. J. Feng, L. Jiang, *Adv. Mater.* **2006**, *18*, 3063–3078.
[4] Y. Tian, B. Su, L. Jiang, *Adv. Mater.* **2014**, *26*, 6872–6897.
[5] R. Wang, K. Hashimoto, A. Fujishima, M. Chikuni, E. Kojima, A. Kitamura, M. Shimohigoshi, T. Watanabe, *Nature* **1997**, *388*, 431–432.
[6] T. Zhang, J. Wang, L. Chen, J. Zhai, Y. Song, L. Jiang, *Angew. Chem. Int. Ed.* **2011**, *50*, 5311–5314; *Angew. Chem.* **2011**, *123*, 5423–5426.
[7] J. Drelich, E. Chibowski, D. D. Meng, K. Terpilowski, *Soft Matter* **2011**, *7*, 9804–9828.
[8] A. K. Geim, K. S. Novoselov, *Nat. Mater.* **2007**, *6*, 183–191.
[9] K. S. Novoselov, V. I. Falko, L. Colombo, P. R. Gellert, M. G. Schwab, K. Kim, *Nature* **2012**, *490*, 192–200.
[10] X. Dong, J. Chen, Y. Ma, J. Wang, M. B. Chan-Park, X. Liu, L. Wang, W. Huang, P. Chen, *Chem. Commun.* **2012**, *48*, 10660–10662.
[11] H.-P. Cong, X.-C. Ren, P. Wang, S.-H. Yu, *ACS Nano* **2012**, *6*, 2693–2703.
[12] H. Bi, X. Xie, K. Yin, Y. Zhou, S. Wan, L. He, F. Xu, F. Banhart, L. Sun, R. S. Ruoff, *Adv. Funct. Mater.* **2012**, *22*, 4421–4425.
[13] Y. Zhao, C. Hu, Y. Hu, H. Cheng, G. Shi, L. Qu, *Angew. Chem. Int. Ed.* **2012**, *51*, 11371–11375; *Angew. Chem.* **2012**, *124*, 11533–11537.
[14] D. D. Nguyen, N.-H. Tai, S.-B. Lee, W.-S. Kuo, *Energy Environ. Sci.* **2012**, *5*, 7908–7912.
[15] Y. Xu, G. Shi, X. Duan, *Acc. Chem. Res.* **2015**, *48*, 1666–1675.
[16] W. Wang, S. Guo, I. Lee, K. Ahmed, J. Zhong, Z. Favors, F. Zaera, M. Ozkan, C. S. Ozkan, *Sci. Rep.* **2014**, *4*, 4452.
[17] Z. Li, Y. Wang, A. Kozbial, G. Shenoy, F. Zhou, R. McGinley, P. Ireland, B. Morganstein, A. Kunkel, S. P. Surwade, L. Li, H. Liu, *Nat. Mater.* **2013**, *12*, 925–931.
[18] J. Rafiee, X. Mi, H. Gullapalli, A. V. Thomas, F. Yavari, Y. Shi, P. M. Ajayan, N. A. Koratkar, *Nat. Mater.* **2012**, *11*, 217–222.
[19] Y. Li, W. Zhou, H. Wang, L. Xie, Y. Liang, F. Wei, J.-C. Idrobo, S. J. Pennycook, H. Dai, *Nat. Nanotechnol.* **2012**, *7*, 394–400.
[20] S. P. Koenig, N. G. Boddeti, M. L. Dunn, J. S. Bunch, *Nat. Nanotechnol.* **2011**, *6*, 543–546.
[21] R. Raccichini, A. Varzi, S. Passerini, B. Scrosati, *Nat. Mater.* **2015**, *14*, 271–279.
[22] D. Li, M. B. Muller, S. Gilje, R. B. Kaner, G. G. Wallace, *Nat. Nanotechnol.* **2008**, *3*, 101–105.
[23] J. Kim, L. J. Cote, J. Huang, *Acc. Chem. Res.* **2012**, *45*, 1356–1364.
[24] B. Samotus, S. Schwimmer, *Nature* **1962**, *194*, 578–579.
[25] A. J. Hatch, J. D. York, *Cell* **2010**, *143*, 1030–1030.
[26] L. Pan, G. Yu, D. Zhai, H. R. Lee, W. Zhao, N. Liu, H. Wang, B. C.-K. Tee, Y. Shi, Y. Cui, *Proc. Natl. Acad. Sci. USA* **2012**, *109*, 9287–9292.
[27] K. Byrappa, T. Adschiri, *Prog. Cryst. Growth Charact. Mater.* **2007**, *53*, 117–166.
[28] J. Shi, H. Wang, K. Schellin, B. Li, M. Faller, J. M. Stoop, R. B. Meeley, D. S. Ertl, J. P. Ranch, K. Glassman, *Nat. Biotechnol.* **2007**, *25*, 930–937.

 © 2016 Wiley-VCH Verlag GmbH & Co. KGaA, Weinheim 

[29] D. Quéré, *Annu. Rev. Phys. Chem.* **2008**, *38*, 71 – 99.
[30] Y.-T. Sul, C. Johansson, A. Wennerberg, L.-R. Cho, B.-S. Chang, T. Albrektsson, *Int. J. Oral Maxillofac. Implants* **2005**, *20*, 349 – 359.
[31] G. Jiang, J. Qiao, F. Hong, *Int. J. Hydrogen Energy* **2012**, *37*, 9182 – 9192.
[32] L. Gao, C. Zhang, M. Zhang, X. Huang, X. Jiang, *J. Alloys Compd.* **2009**, *485*, 789 – 793.
[33] A. Ferrari, J. Meyer, V. Scardaci, C. Casiraghi, M. Lazzeri, F. Mauri, S. Piscanec, D. Jiang, K. Novoselov, S. Roth, *Phys. Rev. Lett.* **2006**, *97*, 187401.
[34] L. G. Cançado, K. Takai, T. Enoki, M. Endo, Y. A. Kim, H. Mizusaki, A. Jorio, L. N. Coelho, R. Magalhães-Paniago, M. A. Pimenta, *Appl. Phys. Lett.* **2006**, *88*, 163106.
[35] S. Crossley, J. Faria, M. Shen, D. E. Resasco, *Science* **2010**, *327*, 68 – 72.
[36] M. P. Ruiz, J. Faria, M. Shen, S. Drexler, T. Prasomsri, D. E. Resasco, *ChemSusChem* **2011**, *4*, 964 – 974.
[37] S. Drexler, J. Faria, M. P. Ruiz, J. H. Harwell, D. E. Resasco, *Energy Fuels* **2012**, *26*, 2231 – 2241.
[38] R. Schlögl, *Angew. Chem. Int. Ed.* **2015**, *54*, 3465 – 3520; *Angew. Chem.* **2015**, *127*, 3531 – 3589.
[39] F. G. Gelalcha, B. Bitterlich, G. Anilkumar, M. K. Tse, M. Beller, *Angew. Chem. Int. Ed.* **2007**, *46*, 7293 – 7296; *Angew. Chem.* **2007**, *119*, 7431 – 7435.
[40] G. Grigoropoulou, J. H. Clark, J. A. Elings, *Green Chem.* **2003**, *5*, 1 – 7.
[41] M. Pera-Titus, L. Leclercq, J.-M. Clacens, F. De Campo, V. Nardello-Rataj, *Angew. Chem. Int. Ed.* **2015**, *54*, 2006 – 2021; *Angew. Chem.* **2015**, *127*, 2028 – 2044.
[42] D. Serrano, R. Sanz, P. Pizarro, I. Moreno, *Chem. Commun.* **2009**, 1407 – 1409.
[43] Z. Shan, Z. Lu, L. Wang, C. Zhou, L. Ren, L. Zhang, X. Meng, S. Ma, F.-S. Xiao, *ChemCatChem* **2010**, *2*, 407 – 412.
[44] L.-H. Chen, X.-Y. Li, G. Tian, Y. Li, J. C. Rooke, G.-S. Zhu, S.-L. Qiu, X.-Y. Yang, B.-L. Su, *Angew. Chem. Int. Ed. Angew. Chem. Int. Ed.* **2011**, *50*, 11156 – 11161; *Angew. Chem.* **2011**, *123*, 11352 – 11357.
[45] W. Lueangchaichaweng, N. R. Brooks, S. Fiorilli, E. Gobechiya, K. Lin, L. Li, S. Parres-Esclapez, E. Javon, S. Bals, G. Van Tendeloo, J. A. Martens, C. E. A. Kirschhock, P. A. Jacobs, P. P. Pescarmona, *Angew. Chem. Int. Ed.* **2014**, *53*, 1585 – 1589; *Angew. Chem.* **2014**, *126*, 1611 – 1615.

Received: November 30, 2015
Revised: January 5, 2016
Published online: February 18, 2016

 © 2016 Wiley-VCH Verlag GmbH & Co. KGaA, Weinheim 